ARTICLES

Scattering of polarized protons from ^{6}Li at 200 MeV

C. W. Glover*
Oak Ridge National Laboratory, Oak Ridge, Tennessee 37831
and Indiana University Cyclotron Facility, Bloomington, Indiana 47405

C. C. Foster and P. Schwandt
Indiana University Cyclotron Facility, Bloomington, Indiana 47405

J. R. Comfort
Physics Department, Arizona State University, Tempe, Arizona 85287

J. Rapaport, T. N. Taddeucci,† and D. Wang‡
Physics Department, Ohio University, Athens, Ohio 45701

G. J. Wagner
Physikalisches Institut der Universität Tübingen, 7400 Tübingen, Germany

J. Seubert
Physics Department, Indiana University-Purdue University at Indianapolis, Indianapolis, Indiana 46223

A. W. Carpenter,§ J. A. Carr, F. Petrovich, R. J. Philpott, and M. J. Threapleton
Physics Department and Supercomputer Computations Research Institute, The Florida State University, Tallahassee, Florida 32306

(Received 11 January 1990)

New cross section and analyzing power data are presented for elastic and inelastic scattering of 200 MeV protons from ^{6}Li. The elastic data are well described by a standard, spherical, 12-parameter phenomenological Woods-Saxon (WS) optical potential. Microscopic folding-model optical potentials, obtained by convoluting free and Pauli-corrected effective nucleon-nucleon (*NN*) interactions with ^{6}Li ground-state densities constrained by electromagnetic data, produce satisfactory descriptions of the elastic data. The effects of the spin-spin optical potential, estimated via the distorted wave approximation (DWA), are small but not negligible. The inelastic transitions leading to the $3^+, T=0$ state at 2.18 MeV and the $0^+, T=1$ state at 3.56 MeV are also examined within the framework of the microscopic folding model using the DWA. Transition potentials are generated by convoluting the two effective *NN* interactions considered with target transition densities constrained by weak and electromagnetic data. These are employed in DWA calculations using both folded optical potentials consistent with the transition potentials and the WS optical potential. The self-consistent calculation with the Pauli-corrected interaction provides a good description of the data for the 3^+ excitation. The results for the 0^+ excitation provide a clear indication that shell model configurations outside the *p* shell are important for a complete description of this transition.

I. INTRODUCTION

This paper presents new cross section and analyzing power data for the elastic and inelastic scattering of 200 MeV protons from ^{6}Li. There have been many earlier studies of this nuclide via elastic and inelastic nucleon[1-10] and electron[11-24] scattering. The nucleon scattering studies were carried out at beam energies ranging from about 20 to 190 MeV, and the data were analyzed at various levels of sophistication. The initial high energy studies[1-5] considered incident protons at 156 and 185 MeV and presented impulse approximation[25] (IA) results based on available electron scattering form factors and free nucleon-nucleon (*NN*) interactions. Both the plane wave (PWIA) and distorted wave impulse approximation (DWIA) were examined, but the estimates of distortion were quite rough.

These studies found that the calculated cross sections for the transitions from the $1^+, T=0$ ground state to the 2.185 MeV $3^+, T=0$ and 3.56 MeV $0^+, T=1$ levels exceeded the experimental data by about a factor of 3 in PWIA and 2 in DWIA. The discrepancies are most clear in the work of Hutcheon, Sundberg, and Tibell,[5] which used the electron scattering form factors directly in the calculations. The work of Refs. 1–4 is based primarily on *LS*-coupled wave functions and certain adjustments, accounting for effects such as quadrupole renormalization,[10] must be made in interpreting the results. The theoretical results for 20 to 50 MeV nucleon scattering[6–8,10] and 136 MeV proton scattering[9] from ^{6}Li, although quite reasonable, are based on somewhat less realistic interactions than the work of Refs. 1–5 and allow no detailed conclusions.

The failure of the DWIA to reproduce the magnitudes of the high energy nucleon scattering cross sections might be attributed to a number of sources, e.g., (i) inadequacies in the single scattering model (i.e., corrections for multiple scattering, coupled channels effects, etc.), (ii) inadequacies in the treatment of the *NN* interaction in the transition matrix elements (i.e., corrections for Pauli blocking and nonlocality in the interaction, accurate treatment of exchange matrix elements, etc.), and (iii) inadequancies in the transition densities employed in the calculations.

Our understanding of nucleon-nucleus scattering at medium energies[26,27] has improved considerably since the work of Refs. 1–10, allowing some assessment of the above points. In regard to (i), the single scattering assumption now appears to be well accepted in the 100–200-MeV incident energy region. This is mainly attributable to the fact that the total *NN* cross section tends toward a minimum of 25 mb at about 200 MeV,[28] as is clear in the graphs of the *NN* *t*-matrix shown in Fig. 7 of both Refs. 26 and 27. Small distortion effects, 33% reduction in the 156 and 185 MeV ^{6}Li cross sections[1–5] and roughly 70% and 50% reductions in 135 MeV ^{28}Si and 200 MeV ^{16}O cross sections[29,30] relative to PW calculations, provide a direct indication of this weak coupling. Finally, explicit estimates of multiple scattering corrections[31] and coupled channels effects[32,33] for nucleon-nucleus scattering in this energy region indicate small effects restricted to large momentum transfers ($q \geq 2$ fm^{-1}).

The most notable recent developments[26,27] for 100–200-MeV nucleon-nucleus scattering concern the properties of the effective *NN* interaction raised in point (ii) above. First, it has been demonstrated that it is essential to include Pauli blocking corrections to the spin-independent central components of the effective *NN* interaction to achieve a quantitative description of scattering observables for elastic scattering and natural parity inelastic transitions[34–37] such as the $1^+, T=0 \rightarrow 3^+, T=0$ transition in ^{6}Li. References 34–37 consider explicitly the targets ^{12}C and ^{16}O. Additional results for ^{16}O are contained in Ref. 30. Second, it has been confirmed that the static, isovector spin-dependent part of the effective *NN* interaction, which is dominant in unnatural parity transitions such as the $1^+, T=0 \rightarrow 0^+, T=1$ transition in ^{6}Li, has the theoretically expected π- and ρ-exchange character.[38] This information has been obtained from the study of forward angle (p,n) reactions[38,39] and studies of stretched excitations in nuclei.[39,40] At present there are a number of available realistic effective *NN* interactions, both of the density-independent, free *t*-matrix type[41] and the density-dependent, *g*-matrix type[42–46] obtained from nuclear matter calculations including Pauli blocking effects. The latter are applied in finite nucleus calculations through the use of the local density approximation[47,34–37] (LDA). Finally, concerning point (iii) above, suffice it to say that the weak and electromagnetic nuclear data base needed to constrain nuclear structure models has improved significantly in recent years.

The present work examines the consequences of points (ii) and (iii) above with respect to new data for scattering of polarized protons from ^{6}Li at an incident laboratory energy of 200 MeV. The experiment is described in Sec. II where angular distributions for both the cross section and analyzing power for elastic scattering and the inelastic transitions leading to the $3^+, T=0$ and $0^+, T=1$ states in ^{6}Li are presented. The study is made within the framework of the single-scattering model. These calculations, described in detail in Sec. III, employ two representations for the effective *NN* interaction. One is the 210-MeV density-independent, free *t*-matrix interaction of Franey and Love[41] and the other is the 200-MeV density-dependent, *g*-matrix interaction of von Geramb[37,45,46] obtained for infinite nuclear matter using the Paris potential.[48] The latter is applied using the LDA.[34–38,47]

The ground-state densities used to construct the optical potential are discussed in Sec. IV A. They consist of a phenomenological spherical density based on the electron scattering data of Li *et al.*[14] and dipole densities constructed from the Cohen-Kurath (CK) spectroscopic amplitudes[49] adjusted to reproduce the static moments[50,51] and transverse electron scattering data of Rand, Frosch, and Yearian[15] and Bergstrom, Kowalski, and Neuhausen.[16] The transition densities used in the inelastic calculations are discussed in Sec. IV B. They are obtained by assuming polynomial Gaussian forms and adjusting the parameters until the weak and electromagnetic transition rates and electron scattering form factor data[17–23,50,51] are reproduced. The present ground state and inelastic transition densities are also compared with those from earlier work in Sec. IV. The results of the nucleon scattering calculations are compared with the new elastic and inelastic data in Sec. V, and Sec. VI contains our conclusions.

II. EXPERIMENT

The data were obtained at the Indiana University Cyclotron Facility (IUCF) using a polarized proton beam at a laboratory bombarding energy of 200.4 MeV. The isotopically enriched, self-supporting ^{6}Li target had a thickness of 29.9 mg/cm^2. The polarization vector of the incident proton beam was oriented normal to the scattering plane and its direction was automatically reversed every 60 sec. The beam polarization was measured periodically

throughout the run using the technique described in Ref. 52; it was typically 75% for each spin orientation.

The scattered protons were momentum analyzed using a quadrupole-dipole-dipole-multipole (QDDM) magnetic spectrometer. The detector assembly in the focal plane included a helical wire gas proportional chamber for position information followed by two plastic scintillators (6.35 mm and 12.7 mm in thickness) for particle identification, also as described in Ref. 52. The beam current and solid angle subtended by the spectrometer were varied such that the dead time for the detector system was less than 10% for all runs except those at the most forward angle, 8° in the laboratory, where it was 35%. The solid angle ranged from 0.1 msr at forward angles to 1.2 msr at the larger angles. The dead time was obtained from the ratio of measured pulser events to generated pulser events using a pulser triggered at a rate proportional to the beam current.

The integrated beam charge for each run was obtained by use of a split Faraday cup internal to the scattering chamber for scattering angles less than 23°, and an external Faraday cup for the larger angles. Since the internal Faraday cup produced incomplete charge integration due to particle outscattering, measurements overlapping in angle were made with both cup configurations. All measurements with the internal cup were then normalized in accordance with the ratio measured to the external cup configuration.

The zero-angle offset of the scattering chamber was found by measuring an angular distribution for the analyzing power over a limited angular range of spectrograph settings to the right and then to the left of the beam. These measurements also allowed us to estimate the uncertainty in scattering angle setting to be ±0.05°.

The energy loss spectrum for 200 MeV spin-up protons on ^{6}Li at 14° in the laboratory is shown in Fig. 1. The yields for the elastic and inelastic data were obtained using the peak-fitting program PEAKFIT.[53] The peaks of interest were fitted with a Gaussian line shape superimposed on a residual linear background.

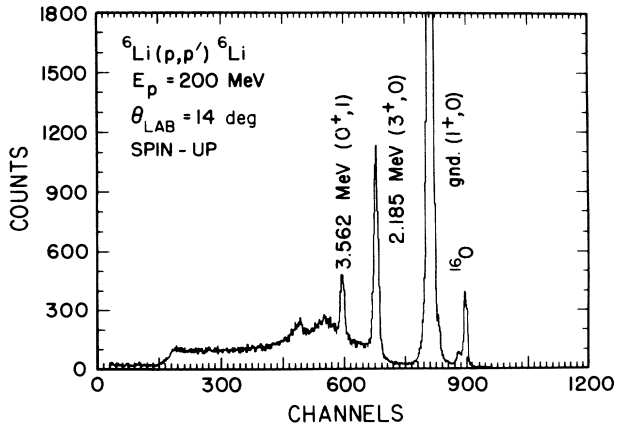

FIG. 1. The energy loss spectrum for 200 MeV spin-up protons scattered from ^{6}Li at an angle of 14° in the laboratory.

The elastic and inelastic $\sigma(\theta)$ and $A_y(\theta)$ are shown as a function of the center-of-mass scattering angle in the figures discussed in Sec. V. The relative uncertainties for the cross section and analyzing power reflect statistical errors as well as uncertainties due to the fitting procedure. The relative error is 2–4% near the peak of the 3^+ angular distribution and 3–7% at the forward angles for the 0^+ state. The forward-most point has a larger error, about 15%, due to uncertainties associated with the large dead-time correction. Not included is the absolute error of ±10% for the elastic and 3^+ cross sections arising from imprecise knowledge of the target thickness. The absolute error increases to ±15% for the 0^+ state due an additional uncertainty in subtracting the underlying nuclear continuum. A complete list of the differential cross sections and analyzing powers for the states measured in this experiment can be obtained from the Physics Auxiliary Publication Service (PAPS).[54]

III. THEORY

A. Single scattering model

The calculations of this work are based on the nonrelativistic microscopic single-scattering model in which the elastic scattering by the spherical part of the ground-state scattering potential (spherical optical potential) is treated exactly; the remaining contributions to elastic scattering (arising from the ^{6}Li ground state spin of 1) as well as inelastic scattering observables are treated perturbatively via the DWA. To make this explicit, with the Hamiltonian for the problem decomposed into relative kinetic energy, target, and projectile-target interaction terms

$$H=\frac{p_r^2}{2\mu}+H_t+\sum_t v_{pt} \tag{1}$$

and the target states defined by

$$H_t|c\rangle=\epsilon_c|c\rangle\ , \tag{2}$$

we write the transition amplitude for nucleon-nucleus scattering in the approximate two potential form[55]

$$T_{eg}=\delta_{eg}\langle\phi_g|U_0(g,g)|\chi_g^{(+)}\rangle + \langle\chi_e^{(-)}|[U(e,g)-\delta_{eg}U_0(g,g)]|\chi_g^{(+)}\rangle\ , \tag{3}$$

where g and e represent ground and excited states, ϕ is a plane wave, U_0 and U are spherical and complete scattering potentials, and the χ's are distorted waves obtained from

$$\left[\nabla^2-\frac{2\mu}{\hbar^2}U_0(c,c)+k_c^2\right]|\chi_c\rangle=0 \tag{4}$$

subject to appropriate scattering boundary conditions. We treat the antisymmetry of the total system wave function required by the Pauli principle by including knockout exchange terms in the scattering potentials[55]

$$U(c',c)=\langle c'|\sum_t v_{pt}(1-P_{pt})|c\rangle\ , \tag{5}$$

where the operator P_{pt} interchanges the coordinates of

the projectile and tth target nucleon. The potentials are thus nonlocal operators in the continuum coordinates. We also employ relativistic kinematics, which are essential for 200-MeV incident nucleons, so μ and k in Eqs. (1) and (4) represent the reduced energy and the wave number corresponding to the momentum of either particle in the nucleon-nucleus center of momentum frame.[56]

It is worthy of note that T_{eg} can be interpreted as an operator in the target and projectile spin spaces. Consistent with this interpretation, the scattering potentials $U(c,c')$ must be regarded as operators in both spin spaces and the wave functions $\chi_g^{(+)}$, etc., must be regarded as operators in the projectile spin space. They are diagonal in the target spin space. In particular, $\chi_g^{(+)}$ would be an operator that describes the spatial evolution of any initial projectile spin orientation under the influence of the spherical part of the scattering potential. We will make use of both the matrix element interpretation implied above and the operator interpretation just described as is convenient.

The effective NN interactions considered[41,37,45,46] are complex, local, energy and density dependent[37,45,46] interactions containing central (C), spin-orbit (LS), and tensor (T) components which can be summarily represented by

$$v_{pt}=v_{pt}[\mathbf{r}_{pt},\mathbf{p}_{pt},\sigma_p,\sigma_t,\rho_g(R),E] , \tag{6}$$

where $\mathbf{r}_{pt}=\mathbf{r}_p-\mathbf{r}_t$ is the NN separation distance, $\mathbf{R}=(\mathbf{r}_p+\mathbf{r}_t)/2$ is the mean position of the NN system, $\mathbf{p}_{pt}$ is the momentum conjugate to $\mathbf{r}_{pt}$, σ_p and σ_t are spin operators, ρ_g is the spherical ground-state matter density, E is the energy used in obtaining v_{pt}, and reference to isospin dependence has been suppressed. In the calculations we treat the exchange nonlocality approximately by invoking short-range limit and asymptotic energy arguments to introduce a modified quasilocal effective NN interaction which, in turn, produces quasilocal scattering potentials, i.e., $v_{pt}(1-P_{pt})\rightarrow\bar{v}_{pt}$ in Eq. (5) and $U_0,U\rightarrow\bar{U}_0,\bar{U}$ in Eqs. (3)–(5).[57–60] The modified interaction $\bar{v}_{pt}$ has nearly the same form as v_{pt} and contains an additional dependence on the wave vector $\mathbf{Q}_0=k_g(\mathbf{k}_e+\mathbf{k}_g)/|\mathbf{k}_e+\mathbf{k}_g|$ characteristic of the exchange process and perpendicular to the momentum transfer $\mathbf{q}=\mathbf{k}_g-\mathbf{k}_e$. Specifically,

$$\bar{v}_{pt}=\bar{v}_{pt}[\mathbf{r}_{pt},\mathbf{p}_{pt},\sigma_p,\sigma_t,\rho_g(R),E,\mathbf{Q}_0] \tag{7}$$

and

$$\bar{U}(c',c)=\langle c'|\sum_t \bar{v}_{pt}|c\rangle . \tag{8}$$

This approximation was first proposed in the IA work of Ref. 25 under the guise of employing symmetrized NN amplitudes evaluated on the nucleon-nucleus energy shell. It neglects coupling to higher order current and spin-current correlations in the target and relative motion.[61] Corrections to the approximation depend on nuclear structure and it is generally found to be very reasonable for most transitions at the energies under consideration here.[61] The $0^+,T=0\rightarrow 1^+,T=1$ transition in ^{12}C represents one particular case where an explicit correction to the approximation is found to be important,[62] as we will discuss later in Sec. V C. A second approximation is to make the LDA[34–37] at the projectile position, i.e., $\rho_g(R)\rightarrow\rho_g(r_p)$ in Eqs. (6) and (7). This greatly simplifies the calculation of the scattering potentials defined in Eqs. (5) and (8). The uncertainties in this procedure are expected to be of the same order as those in the LDA itself, given the relatively short range of the NN interaction. A systematic study of corrections to the LDA due to the local rate of change of the nuclear density has not been made.

With the above approximations, the calculations are executed by decomposing the interaction $\bar{v}_{pt}$ into multipoles, performing the integration over target coordinates in Eq. (8) to obtain the scattering potentials, and employing these potentials as prescribed by Eqs. (3) and (4). The multipole decomposition is most easily obtained by employing the finite momentum space and Cartesian tensor techniques of Refs. 63 and 64. The resulting expansion can be written in the compact form

$$\bar{v}_{pt}=\sum_{n,\alpha\beta} w_n^2\bar{v}_{pt}^{\beta\alpha}(k_n)\mathcal{T}_J^{\beta}(p)\cdot\mathcal{T}_J^{\alpha}(t) , \tag{9}$$

where the $\mathcal{T}_J^{\nu}(i)$ are Cartesian tensors measuring matter ($\nu=m$), transverse current ($l\perp$), diagonal spin (s), spin-current (ls), transverse and longitudinal spin ($s\perp$ and $s\parallel$), and diagonal current (l) correlations in the projectile ($i=p$), and target ($i=t$), $\bar{v}_{pt}^{\beta\alpha}(k_n)$ is the Bessel transform of the interaction component coupling β projectile and α target correlations taken with respect to r_{pt}, and $w_n^2=(2/\pi)k_n^2\Delta k_n$ are the Fourier-Bessel weights defined for a sphere of radius $R_M\sim 12$ fm. Substituting Eq. (9) into Eq. (8) and expressing the result as an operator in the spin space of the target yields

$$\bar{U}(c',c)=\sum_J \hat{J}^{-1}\bar{U}_J(c',c)\cdot\tau_{c'c}^J , \tag{10}$$

where $\hat{J}=\sqrt{2J+1}$, the $\tau_{c'c}^J$ are statistical tensors or statistical transition tensors,[55] and the $\bar{U}_J(c',c)$ are the multipole scattering potentials given by

$$\bar{U}_{JM_J}(c',c)=\sum_{n,\beta\alpha} w_n^2\mathcal{T}_{JM_J}^{\beta}(p)\bar{v}^{\beta\alpha}(k_n)\rho_J^{\alpha}(c',c;k_n) \tag{11}$$

with

$$\rho_J^{\alpha}(c',c;k_n)=\langle c'\|\sum_t \mathcal{T}_J^{\alpha}(t)\|c\rangle \tag{12}$$

representing the target transition densities. For further details the reader is referred to Ref. 64, in particular Table I and Appendix B. Additional information is contained in Ref. 32. To make contact here with the more common coordinate space convolution expressions for the scattering potentials, we note that for $c'=c=g$, $J=M_J=0$, and $\rho_0^{ls}=0$, it is easy to show that Eq. (11) is equivalent to the usual central plus spin-orbit expression for the spherical optical potential, i.e.,

$$\bar{U}_0(g,g)\equiv\bar{U}_{00}(g,g)$$
$$=\int \bar{v}^{\,C}(r_{pt})\rho_g(r_t)d^3r_t$$
$$+\int \bar{v}^{\,LS}(r_{pt})\mathbf{r}_{pt}\rho_g(r_t)d^3r_t\times\mathbf{p}_p\cdot\boldsymbol{\sigma}_p \qquad (13)$$

with $\rho_g=(4\pi)^{-1/2}\rho_0^m$.

Explicit expressions for the transition amplitudes are obtained using Eq. (10) in Eq. (3) which yields

$$T_{eg}=\sqrt{2}\sum_J \beta_J(e,g)\cdot\tau_{eg}^J\ , \qquad (14)$$

where β_J is a matrix in the projectile spin space with elements given by

$$\beta_{JM_J}(e,g)=(\sqrt{2}\hat{J})^{-1}\begin{cases}\langle\phi_g|\bar{U}_0(g,g)|\chi_g^{(+)}\rangle \quad (e=g,\ J=0)\ , & (15a)\\ \langle\chi_e^{(-)}|\bar{U}_{JM_J}(e,g)|\chi_g^{(+)}\rangle \quad \text{(otherwise)}\ . & (15b)\end{cases}$$

This can alternatively be written in terms of distortion functions as

$$\beta_{JM_J}(e,g)=\sum_{n,\beta} w_n^2 D^{\beta}_{JM_J}(k_n,\theta)\bar{U}^{\,\beta}_J(k_n) \qquad (16)$$

with the distortion elements.

$$D^{\beta}_{JM_J}(k_n,\theta)=(\sqrt{2}\hat{J})^{-1}\begin{cases}\langle\phi_g|\mathcal{T}^{\beta}_{00}(p)|\chi_g^{(+)}\rangle\ , & (17a)\\ \langle\chi_e^{(-)}|\mathcal{T}^{\beta}_{JM_J}(p)|\chi_g^{(+)}\rangle\ . & (17b)\end{cases}$$

For the case of density independent interactions, i.e., $\bar{v}^{\,\beta\alpha}$ not parametrically dependent on r_p, we have

$$\bar{U}^{\,\beta}_J(k_n)=\sum_\alpha \bar{v}^{\,\beta\alpha}(k_n)\rho^\alpha_J(k_n)\ . \qquad (18)$$

For density dependent interactions $\bar{U}^{\,\beta}_J(k_n)$ must be constructed by explicitly Fourier transforming the left-hand side of Eq. (11). The details of this procedure are unimportant here.

The differential cross sections $\sigma(\theta)$ and analyzing powers $A_y(\theta)$ are obtained from Eq. (14) in the usual way:[55]

$$\sigma(\theta)=\left[\frac{\mu}{2\pi\hbar^2}\right]^2\frac{k_e}{k_g}\frac{1}{2(2J_g+1)}\mathrm{Tr}(TT^\dagger)\ , \qquad (19)$$

$$A_y(\theta)=\mathrm{Tr}(T\sigma_{py}T^\dagger)/\mathrm{Tr}(TT^\dagger)\ , \qquad (20)$$

where J_g is the ground-state spin and we have dropped the channel labels e and g on σ, A_y, and T for convenience. Since the spin of the target is not observed, σ and A_y can be written as incoherent sums of partial cross sections $\sigma^J(\theta)$ and analyzing powers $A_y^J(\theta)$ corresponding to definite total angular momentum transfer J between the projectile and target, i.e.,

$$\sigma(\theta)=\sum_J \sigma^J(\theta) \qquad (21)$$

and

$$A_y(\theta)=\sum_J A_y^J(\theta)\ . \qquad (22)$$

The $\sigma^J(\theta)$ and $A_y^J(\theta)$ are obtained from analogs of Eqs. (19) and (20) with β_J appearing in place of T.

To gain some feeling for the full detail of the scattering calculations, it is useful to make the Born approximation [$D\sim\delta(k_n-q)/k_nq$ in Eq. (16)] and neglect the density dependence in the NN interaction [$\bar{U}^{\,\beta}_J=\sum_\alpha\bar{v}^{\,\beta\alpha}\rho^\alpha_J$ as in Eq. (18)] to obtain compact explicit expressions for the $\sigma^J(\theta)$.[27] Using N for natural parity [$\Delta\pi=\pi_i\pi_f=(-1)^J$ for the target] and U for unnatural parity [$\Delta\pi=(-1)^{J+1}$] these are

$$\sigma^J_N(\theta)=4\pi\left[\frac{\mu}{2\pi\hbar^2}\right]^2\frac{(2J_e+1)}{(2J_g+1)}(|\bar{t}_m\rho^m_J|^2+|\bar{t}_{ls}\rho^{ls}_J|^2+I_{m,ls}+|\bar{t}_{s\perp}\rho^s_J|^2+|\bar{t}_{l}\rho^{l\perp}_J|^2+I_{s,l\perp}) \qquad (23a)$$

and

$$\sigma^J_U(\theta)=4\pi\left[\frac{\mu}{2\pi\hbar^2}\right]^2\frac{(2J_e+1)}{(2J_g+1)}(|\bar{t}_{s\parallel}\rho^{s\parallel}_J|^2+|\bar{t}_{s\perp}\rho^{s\perp}_J|^2+|\bar{t}_{l}\rho^{l}_J|^2+I_{s\perp,l})\ , \qquad (23b)$$

where the $\bar{t}_\alpha$ are combinations of the components of $\bar{v}$ and the Born approximation D representing the coupling to a given ρ^α ($\bar{t}_\alpha=\sum_\beta D^\beta\bar{v}^{\,\beta\alpha}$) and the I represent interference terms. The matter term is dominant for the natural parity case in Eq. (23a) and the longitudinal and transverse spin terms are most important for the unnatural parity case of Eq. (23b). The former comes from the spin-independent central and spin-orbit components of the NN interaction, while the latter come from the spin-dependent central and tensor interaction components. With suitable specification of the $\bar{t}_\alpha$, Eqs. (23a) and (23b) can be used to represent electron-nucleus scattering cross sections.[27] In particular, the first three terms in Eq. (23a) are related to the longitudinal form factor, the remaining

three are related to the transverse electric form factor (which vanishes for elastic scattering), and Eq. (23b) is related (with $\bar{t}_{s\|}=0$) to the transverse magnetic form factor. Equivalent formulas, in more conventional notation, are given in Sec. 4 of Ref. 64.

In the calculations to be discussed below, the scattering potentials defined in Eq. (11) are constructed using the computer code ALLWRLD.[65] These are used as input to the DWA code TAMVAX[66] where the projectile matrix elements defined in Eq. (15) are evaluated to form the transition amplitude and calculate cross sections and analyzing powers. We also use the code EFIT[67] to adjust densities to fit electron scattering data.

B. Interactions

Two forms for the effective *NN* interaction are used in the calculations. One is the 210-MeV free *t*-matrix interaction of Franey-Love[41] which is density independent. The other consists of the 200-MeV density-dependent *g*-matrix interaction of von Geramb[37,45,46] based upon the Paris potential.[48]

The differences between these two effective *NN* interactions will be reflected mainly in the calculated observables for the elastic scattering and natural parity transitions. These transitions are primarily driven by the spin-independent *C* and *LS* components of the *NN* interaction. It is the spin-independent *C* components of the *NN* interaction that are most sensitive to the Pauli corrections.[35,68,69] Specifically, concentrating on the isoscalar spin-independent *C* component, the real part of the density-dependent interaction becomes less attractive (more repulsive) at low q (high q) than the free interaction as the density increases. Correspondingly, the zero for the density-dependent interaction occurs at smaller momentum transfer for higher densities. The imaginary part of this component of the density-dependent interaction is much less absorptive at low q for high density. The interested reader is referred to Figs. 6 and 7 in Ref. 68 for typical results at 140 MeV. Correspondingly, the cross-section calculations for these transitions using the density-dependent interaction are expected to be smaller at low q and larger at high q than those using the free interaction. Furthermore, the shift to lower q in the zero of the density-dependent *C* interaction component will be reflected by a similar shift in the zero of the analyzing power.[70]

The isovector spin-dependent *C* and *T* interaction components have π- and ρ-exchange character[38–40] and are relatively unaffected by Pauli corrections. Hence, there should not be much difference between the calculations for unnatural parity transitions using the two interactions.

IV. NUCLEAR DENSITIES

All of the nuclear structure information of interest for the scattering calculations is contained in the target densities. Much of the work on ^{6}Li cited in Refs. 1–24 is based on the *LS*-coupling harmonic oscillator shell model. In the *LS* model, it is assumed that ^{6}Li has an inert α-particle core with two valence nucleons restricted to the $1p$ shell. The $1^+,T=0$ ground state and $3^+,T=0$ and $0^+,T=1$ excited states are described by the $^{13}S_1$, $^{13}D_3$, and $^{31}S_0$ configurations, respectively. The densities obtained from these wave functions serve as a useful point of reference for the discussion below.

An important feature of the shell model with valence particles restricted to the p shell is that the dominant densities ρ_J^m, $\rho_J^{s\|}$, $\rho_J^{s\perp}$ as well as ρ_J^s and ρ_J^l are completely characterized by three shape functions. Specifically,

$$\rho_J^\alpha=\delta_{J0}S_J^\alpha\langle j_J\rangle_s+P_J^\alpha\langle j_J\rangle_p \tag{24}$$

for $\alpha=m,s$ and $J=0,2$. Further, with $\rho_J^{s\perp}$, $\rho_J^{s\|}$, and ρ_J^l decomposed into $L=J\pm1$ components according to Table I and Eq. (A7) of Ref. 64:

$$\rho_J^{s\perp}=\left[\frac{J+1}{2J+1}\right]^{1/2}\rho_{J,J-1}^s-\left[\frac{J}{2J+1}\right]^{1/2}\rho_{J,J+1}^s\,, \tag{25a}$$

$$\rho_J^{s\|}=\left[\frac{J}{2J+1}\right]^{1/2}\rho_{J,J-1}^s+\left[\frac{J+1}{2J+1}\right]^{1/2}\rho_{J,J+1}^s\,, \tag{25b}$$

$$\rho_J^l=-[J(J+1)]^{-1/2}\left[\left[\frac{J}{2J+1}\right]^{1/2}\rho_{J,J-1}^{\bar{l}}+\left[\frac{J+1}{2J+1}\right]^{1/2}\rho_{J,J+1}^{\bar{l}}\right], \tag{25c}$$

we have

$$\rho_{JL}^\alpha=P_{JL}^\alpha\langle j_L\rangle_p \tag{26}$$

for $\alpha=s,\bar{l}$, $J=1,3$, and $L=0,2$. For harmonic oscillator radial wave functions, the three shape factors are

$$\langle j_0\rangle_s=e^{-x}\,, \tag{27a}$$

$$\langle j_0\rangle_p=(1-\tfrac{2}{3}x)e^{-x}\,, \tag{27b}$$

$$\langle j_2\rangle_p=\tfrac{2}{3}xe^{-x}\,, \tag{27c}$$

with $x=k_n^2/4\alpha^2$ and $\alpha=(M\omega/\hbar)^{1/2}$ representing the oscillator size parameter. We also note that

$$P_{10}^{\bar{l}}=\sqrt{2}\,P_{12}^{\bar{l}} \tag{28}$$

within the p-shell model. Additional shape factors are necessary to describe the densities ρ_J^{ls} and $\rho_J^{l\perp}$ which are expectations of operators involving radial derivatives. These are not important for the present application and will not be discussed here.

The first term in Eq. (24) constitutes the contribution of the α-particle core to the ground-state densities, with $S_0^m=1.126$ and $S_0^s=0$ independent of coupling scheme. The values of P_J^α and P_{JL}^α obtained from the *LS*-coupling shell model for the three transitions of interest in ^{6}Li are summarized in Table I. Also shown, as a second entry, are the values corresponding to the intermediate coupling model of Cohen and Kurath.[49] These are, for the most part, quite close to the *LS*-coupling values. The P_J^α and P_{JL}^α, which have been taken from Table 2 of Ref. 10, succinctly display the basic character of each transition.

Deficiencies in these model densities associated with limitations in the shell model vector space can be corrected for, in part, by adjusting the densities to reproduce weak-interaction and electromagnetic data. This is most easily done by introducing scale factors Δ_J^α and Δ_{JL}^α corresponding to the densities in Eqs. (24) and (26) and varying these along with the oscillator size parameter to fit the selected data. The use of the Δ^α may be viewed as redefining the P^α. One of the earliest applications of this procedure was due to Griffy and Yu.[71] The fitted parameters for ^{6}Li, first suggested in Ref. 8 and modified in Ref. 10, are summarized in the footnotes to Table I. Unless otherwise noted, all values given here are intended for use in calculations in which the standard finite nucleon size[72] and center-of-mass corrections[73] are applied explicitly to ρ_J^α and ρ_{JL}^α as described in Ref. 64. The corresponding fits to electron scattering are shown as dot-dashed curves in Figs. 2 and 3 to be discussed below. We now turn to the discussion of the improved densities used in the present nucleon scattering calculations.

A. Ground state densities

The ground state of ^{6}Li has spin and parity 1^+ and isospin zero. Consequently, there are spherical ($J=0$), dipole ($J=1$), and quadrupole ($J=2$) isoscalar densities that must be determined. Since the measured[50,51] quadrupole moment of ^{6}Li is very small ($Q_2=-0.0644\pm0.0007$ e fm^2) we assume that all of the $J=2$ ground state densities vanish. This is consistent with the LS-coupling wave functions but not the intermediate coupling wave functions, which predict a large ground state ρ_2^m and correspondingly a large Q_2.

The best fit to the longitudinal elastic electron scattering form factor data of Refs. 13 and 14 using the shell model ρ_0^m requires $\alpha_s\neq\alpha_p$ and is shown as a dot-dashed curve in Fig. 2(a). LS and intermediate coupling wave functions are equivalent for this density. The result clearly fails to describe the data beyond $q\approx2.0$ fm^{-1}. In this model, no improvement can be obtained for $q\geq2.0$ fm^{-1} without sacrificing the quality of the fit at lower q. Li *et al.*[14] introduced the density

$$\rho_{\rm ch}(q)=e^{-a^2q^2}-c^2q^2e^{-b^2q^2}+de^{-(q-q_0)^2/p^2} \tag{29}$$

with $a=0.928$ fm, $b=1.26$ fm, $c=0.48$ fm, $d=-0.00124$, $q_0=3.11$ fm^{-1}, and $p=0.70$ fm^{-1} to achieve the fit indicated by the solid curve in Fig. 2(a). This result is in excellent agreement with the experimental data out to $q\approx3.7$ fm^{-1}. For the present calculation

TABLE I. The P_J^α and P_{JL}^α coefficients of Eqs. (24) and (26) for the three transitions in ^{6}Li under consideration. The first entry corresponds to the LS-coupling model and the second is for the intermediate coupling CK model. The column headings specify the transition, total angular momentum transfer J, and the superscript α on P. The symbols < and > refer to $L=J-1$ and $L=J+1$.

$(J_i^\pi;T_i)\rightarrow(J_f^\pi;T_f)$	J	m	s	$s_<$	$s_>$	$\bar{l}_<$	$\bar{l}_>$
$(1^+;0)\rightarrow(1^+;0)$	0[a]	0.564	0				
		0.564	0				
	1[b]			0.798	0	0	0
				0.701	0.084	0.048	0.034
	2	0	0				
		−0.209	0				
$(1^+;0)\rightarrow(3^+;0)$	2[c]	−0.357	−0.291				
		−0.364	−0.311				
	3			−0.412	0	0	0
				−0.382	0	0	0
$(1^+;0)\rightarrow(0^+;1)$	1[d]			0.977	0	0	0
				0.937	−0.167	0.068	0.048

[a]Suelzle *et al.* (Ref. 13), Bray *et al.* (Ref. 8), and Petrovich *et al.* (Ref. 10) have reported that the longitudinal elastic electron scattering form factor can be described out to $q\approx2.0$ fm^{-1} with $\Delta_0^m=1.0$, $\alpha_s=0.613$ fm^{-1}, and $\alpha_p=0.505$ fm^{-1}. These values are based on fits to the experimental data of Ref. 13.

[b]Bray *et al.* (Ref. 8) and Petrovich *et al.* (Ref. 10) have reported that the transverse elastic electron scattering form factor can be described by the LS-coupled wave functions with $\Delta_{10}^s=0.934$ and $\alpha_p=0.577$ fm^{-1}. These values are based on fits to the experimental data of Ref. 15 which extend only to $q\approx1.4$ fm^{-1}. Note that the theoretical curve corresponding to this result in Fig. 3 of Ref. 10 is in error.

[c]Bray *et al.* (Ref. 8) have reported that the experimental longitudinal inelastic electron scattering form factor data of Ref. 11 for the excitation of the $3^+,T=0$ state can be described by the LS-coupled wave function with $\Delta_2^m=1.93$ and $\alpha_p=0.488$ fm^{-1}. Petrovich *et al.* (Ref. 10) reported that the newer data of Refs. 17–20 and 23 required $\Delta_2^m=1.69$ and was only roughly described out to $q\approx2.0$ fm^{-1} with $\alpha_p=0.448$ fm^{-1}.

[d]Bray *et al.* (Ref. 8) have reported that the experimental transverse inelastic scattering form factor data of Ref. 12 for the excitation of the $0^+,T=1$ state can be described by the LS-coupled wave function with $\Delta_{10}^s=1.03$ and $\alpha_p=0.518$ fm^{-1} without inclusion of the center-of-mass correction. The experimental data of Ref. 12 extends only to $q\approx1.2$ fm^{-1} and is sensitive to the center-of-mass correction. Petrovich *et al.* (Ref. 10) reported that the newer data of Refs. 21–23 required $\Delta_{10}^s=1.00$ and was only well described by these parameters for $q\leq0.8$ fm^{-1}. The LS-coupling results we show here are based on the latter parameters with the center-of-mass correction included.

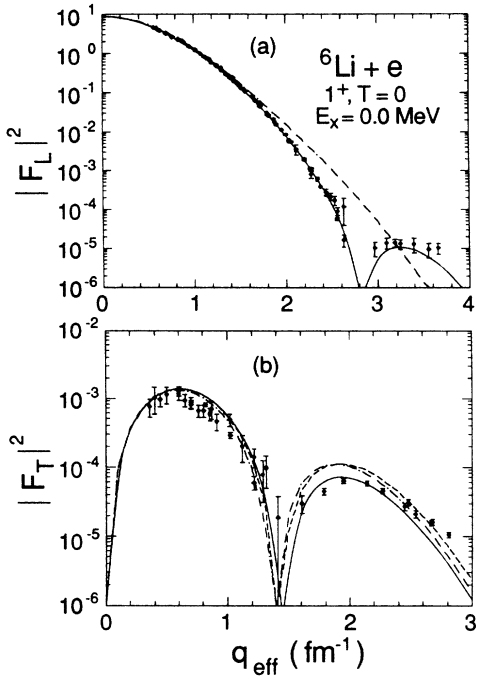

FIG. 2. Electron scattering form factors calculated from densities used in the proton scattering calculations are compared with (a) the longitudinal elastic data of Refs. 13 and 14 and (b) the transverse elastic data of Refs. 15 and 16. The dot-dashed curves are calculated using the densities from Refs. 8 and 10 based on old electromagnetic data of Refs. 11–13. The solid curves are the results obtained using densities that have been adjusted to reproduce the more recent and complete weak and electromagnetic data base considered here. One intermediate result is shown as a dashed curve. See the text for details.

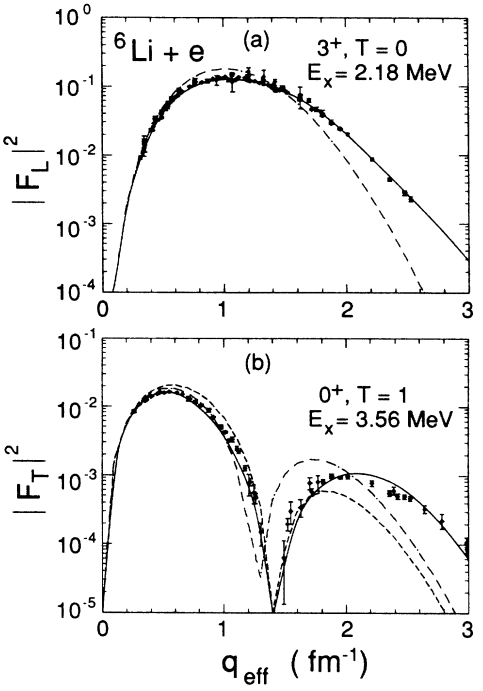

FIG. 3. Same as Fig. 2 for (a) the longitudinal inelastic 3^+ data of Refs. 17, 19, 20, and 23 and (b) the transverse inelastic 0^+ data of Refs. 21–23.

we construct ρ_g from $\rho_{\rm ch}$ by invoking charge symmetry to assert $\rho^m_{0p}=\rho^m_{0n}$ and deconvoluting the finite proton and neutron size according to

$$\rho_g=\frac{2\rho_{\rm ch}}{\rho^e_p+\rho^e_n}\ . \tag{30}$$

No center-of-mass correction is to be made with this density.

The $J=1$ transverse magnetic elastic electron scattering form factor for the LS-coupling model result of Refs. 8 and 10 is shown as a dot-dashed curve in Fig. 2(b) and compared with the experimental data of Rand, Frosch, and Yearian[15] and Bergstrom, Kowalski, and Neuhausen.[16] This result is consistent with the experimental magnetic moment ($\mu=0.822$ nm). Agreement with the data can be improved slightly by changing α_p from 0.577 fm^{-1} to 0.564 fm^{-1} as indicated by the dashed curve in Fig. 2(b). A nearly equivalent fit is obtained with the CK wave functions[49] using the same size parameter $\alpha_p=0.564$ fm^{-1} and $\Delta^s_{10}=\Delta^s_{12}=\Delta^{\bar{I}}_{10}=\Delta^{\bar{I}}_{12}=0.986$. Further improvement can be made at high q by renormalizing the $L=2$ densities. The final result is shown as the solid curve in Fig. 2(b). Since the electron scattering data does not distinguish between the spin and convection current densities, aside from small effects due to differences between nucleon form factors, the final fit strictly yields only the conditions

$$\Delta^s_{10}+0.077\Delta^{\bar{I}}_{10}\approx 1.061\ , \tag{31a}$$

$$\Delta^s_{12}-1.300\Delta^{\bar{I}}_{12}\approx -1.499\ , \tag{31b}$$

whose left-hand sides are easily inferred from Eqs. (72a) and (72b) in Ref. 64 and the density coefficients in Table I.

For lack of further information, in the present calculations we make the choice $\Delta^s_{10}=\Delta^{\bar{I}}_{10}=\Delta^{\bar{I}}_{12}=0.986$ and $\Delta^s_{12}=-0.217$, i.e., we reduce the model current and $L=0$ spin densities by a constant factor to reproduce the experimental magnetic moment and adjust the model $L=2$ spin density to reproduce the second peak in the experimental form factor. To investigate the sensitivity of the proton scattering results to these assumptions, we have made additional calculations with $\Delta^s_{10}=\Delta^{\bar{I}}_{10}=0.986$, $\Delta^s_{12}=1.00$, and $\Delta^{\bar{I}}_{12}=1.92$ which also satisfy Eq. (31). With this choice we are holding the model spin densities nearly fixed and invoking corrections to the model current densities which must be attributed to shell model configurations outside the p shell since the adjusted $P^{\bar{I}}_{JL}$ violate the condition in Eq. (28). This is not unreasonable since the effects we are trying to mimic using the Δ normalization factors involve excitations out of the p shell.[74] It is not our intent to discuss these effects here, but rather to investigate the sensitivity of proton scattering results to two quite distinct choices for the $L=2$ densities. The

second choice yields proton scattering results which deviate minimally from the intermediate coupling model since proton scattering is most sensitive to the spin densities.

B. Transition densities

The longitudinal inelastic electron scattering form factor for the $1^+,T=0\rightarrow 3^+,T=0$ ($E_x=2.184$ MeV) transition in ^{6}Li using the *LS*-coupling model result of Ref. 10 is shown as a dot-dashed curve and compared with the experimental data of Refs. 17, 19, 20, and 23 in Fig. 3(a). This is clearly too high at the peak and inadequate for $q\geq 2.0$ fm^{-1}. An improved quadrupole matter transition density was found phenomenologically by assuming a polynomial Gaussian expansion (PGE) given in momentum space by

$$\rho_2^m(q)=\left[\frac{3}{7\pi}\right]^{1/2}\exp\left[\frac{-q^2}{4\alpha^2}\right]\sum_{n=1}^{5}a_{2n}q^{2n}\ . \tag{32}$$

The coefficients a_{2n} and the oscillator constant α were varied until a fit to the 3^+ longitudinal electron scattering form factor data was obtained with the γ-transition rate fixed at the experimental value[18] [$B(E2\uparrow)=(23.5\pm 1.8)e^2$ fm^4]. Five terms in the sum were sufficient for an excellent fit to the data. The resulting coefficients and oscillator constant are given in Table II. The longitudinal inelastic electron scattering form factor generated from this phenomenological density is shown as the solid curve in Fig. 3(a); it reproduces the data over the full range of momentum transfer. The transverse form factor for the $1^+,T=0\rightarrow 3^+,T=0$ ($E_x=2.184$ MeV) transition in ^{6}Li is very small[11,14,18,20] and we assume that the spin and current densities contributing to the $E2$ and $M3$ amplitudes are negligible.

Finally, the transverse inelastic electron scattering form factor for the $1^+,T=0\rightarrow 0^+,T=1$ ($E_x=3.56$ MeV) transition in ^{6}Li using the *LS* coupling model result of Refs. 8 and 10 is shown as a dot-dashed curve and compared with the experimental data of Refs. 21–23 in Fig. 3(b). This result is consistent with the experimental electromagnetic transition rate[18] [$B(M1\uparrow)=0.059e^2$ fm^2], but it is quite inadequate in describing the form factor data in the region of the minimum and beyond. Furthermore, the result is not consistent with the ^{6}He(β^-)^{6}Li decay rate[50] ($\langle GT\rangle^2=4.87$ using $\langle F\rangle^2+1.56\langle GT\rangle^2=6163$/ft from Ref. 75). The latter problem can be remedied by introducing the CK wave functions[49] and fixing $\Delta_{10}^s=0.939$ and $\Delta_{10}^I=6.68$ to reproduce simultaneously the weak and electromagnetic transition rates. The q dependence of the electromagnetic form factor is another matter.

To be more specific we note that it is not possible to obtain a good fit to the experimental electromagnetic form factor data over the entire q range by varying the $L=2$ renormalization factors and the oscillator size parameter. Bergstrom, Auer, and Hicks[22] have reported that a good fit to the low-q data can be obtained with $\alpha_p=0.463$ fm^{-1}. However, this fit badly underestimates the second peak in the form factor. A careful comparison of the experimental elastic transverse form factor shown in Fig. 2(b) and transverse form factor data for the 0^+ excitation in Fig. 3(b) (including the $q=0$ point) suggests that a fit favoring the high-q data can be obtained with $\alpha_p=0.564$ fm^{-1}. Unfortunately, this fit significantly overestimates the first peak in the form factor data. Given this state of affairs we will present results with $\alpha_p=0.518$ fm^{-1}, i.e., the value deduced in the earlier work of Refs. 8 and 10 and intermediate to the extreme values mentioned above. With this value of the oscillator size parameter, the best compromise fit to the electromagnetic form factor data is achieved with

$$\Delta_{12}^s+0.173\Delta_{12}^I\approx 2.118\ . \tag{33}$$

With $\Delta_{12}^I=6.68$ as required by the p-shell model, Eq. (33) yields $\Delta_{12}^s=0.963$. This result is shown as a dashed curve in Fig. 3(b).

To gain any further improvement, it is necessary to relax the condition of harmonic oscillator radial wave functions, the restriction to the p shell, or both. Bergstrom

TABLE II. The oscillator constants and expansion coefficients obtained for the phenomenological transition density and p-shell radial wave function defined in Eqs. (32) and (34), respectively.

$(J_i^\pi;T_i)\rightarrow(J_f^\pi;T_f)$	α	a_2	a_4	a_6	a_8	a_{10}
$(1^+;0)\rightarrow(3^+;0)$	0.4774	1.14	-0.407	0.335	-6.84×10^{-2}	6.44×10^{-3}
	α	a_2	a_3	a_4	a_6	a_8
$(1^+;0)\rightarrow(0^+;1)$	0.430[a]	1.063×10^{-1}	-5.091×10^{-2}	8.433×10^{-3}	-1.126×10^{-4}	1.407×10^{-6}
	0.495[b]	6.625×10^{-2}		-5.036×10^{-3}	1.967×10^{-4}	
	0.4958[c]	7.40×10^{-2}		-6.80×10^{-3}	2.78×10^{-4}	

[a]Reference 23.
[b]Reference 76.
[c]Present work.

and co-workers[22,23] have investigated the foremost of these possibilities using p-shell model amplitudes based on fits to μ, Q_2, $\langle r^2\rangle_p$, and $B(M1\uparrow)$ for ^{6}Li and a p-shell radial wave function of polynomial Gaussian form

$$[R(r)]^2=e^{-(\alpha r)^2}\sum_n a_n r^n \ . \tag{34}$$

The resulting density coefficients for the $1^+\rightarrow 0^+$ transition are $P^s_{10}=0.880$, $P^s_{12}=0.120$, $P^{\bar{I}}_{10}=0.454$, and $P^{\bar{I}}_{12}=0.321$; the corresponding a_n coefficients are given in Table II. These densities are found to be consistent with the experimental $\langle GT\rangle^2$, which was not included in the fit. Note further that the fit of Ref. 23 contains a term with odd integer n that does not follow from an expansion in oscillators. Kiziah *et al.*[76] have adopted a similar point of view in a study of the excitation of the $0^+,T=1$ level in ^{6}Li via 100–260-MeV pions. They made a fit to the inelastic electron scattering form factor, ignoring the experimental $\langle GT\rangle^2$ and assuming $P^s_{10}=0.977$, $P^s_{12}=0.073$, and $P^{\bar{I}}_{10}=P^{\bar{I}}_{12}=0$ with only even integer n in the expansion of Eq. (34). The resulting parameters are also given in Table II. The electromagnetic data alone strictly determines only

$$-1.918P^s_{10}-0.408P^{\bar{I}}_{10}\approx 1.873 \ , \tag{35a}$$

$$1.357P^s_{12}-0.816P^{\bar{I}}_{12}\approx -0.099 \ . \tag{35b}$$

We have made a third fit, assuming the P^{α}_{JL} of Ref. 23 and even integer n, using the code EFIT.[67] The resulting parameters are listed in Table II with those of Refs. 23 and 76. The fits to the inelastic transverse form factor corresponding to Refs. 23, 76, and this paper are similar, and we show only the present results as a solid curve in Fig. 3(b).

In closing this section we reemphasize that the electron and pion scattering data, which are primarily determined by $\rho^{s\perp}_1$, do not test the assumption that $\langle j_0\rangle_p$ and $\langle j_2\rangle_p$ are related through common radial wave functions which has been made in describing all of the sets of dipole densities discussed above. Nucleon scattering depends mainly on both $\rho^{s\perp}_1$ and $\rho^{s\parallel}_1$, so a combination of electron scattering and nucleon scattering data does provide information on this point. This has been discussed in several places,[26,27,32,39,40] most recently in Ref. 77.

V. PROTON SCATTERING RESULTS

A. Elastic scattering

The elastic scattering differential cross section and analyzing power data are shown in Figs. 4 and 5. These

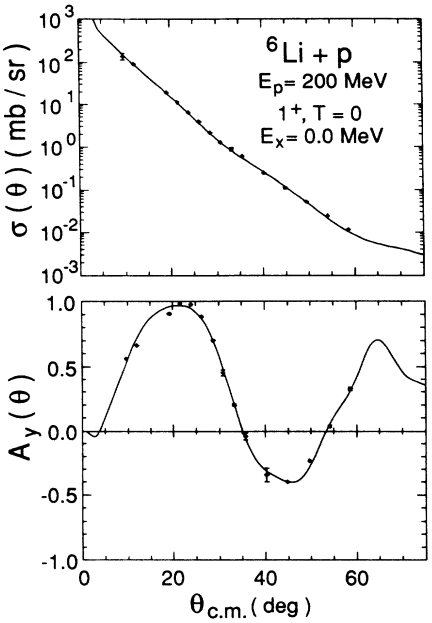

FIG. 4. The result of a calculation using a phenomenological WS optical potential that was adjusted to fit the present elastic scattering cross section and analyzing power data is shown.

data were first fit to obtain empirical optical model parameters in the usual way,[78] by adjusting Woods-Saxon (WS) potentials until acceptable agreement with the data was obtained. The computer code SNOOPY[79] was used to execute this procedure. An integration step size of 0.1 fm, Coulomb matching radius of 10.5 fm, and 30 partial waves were used in these calculations. The resulting 12 parameters WS optical potential set is given in Table III. The fit to the data is shown in Fig. 4. The phenomenological optical potential gives an excellent reproduction of the elastic data. It must be noted that this fit is made without any reference to the spin-spin potential ($J=1$) for ^{6}Li and any effects due to this potential are subsumed into the resulting parameters.

The results of the microscopic calculations for elastic scattering based on the t- and g-matrix interactions are shown in Figs. 5(a) and 5(b), respectively. The $J=0$ partial cross sections and analyzing powers, σ^0 and A^0_y, obtained by solving the Schrödinger equation [Eq. (4)] with the spherical folded potentials $\bar{U}_0(g,g)$ [Eq. (13)] constructed from the $J=0$ ground-state densities given in Sec. IV A are shown as short dashed curves. The $J=1$

TABLE III. The WS optical potential[a] parameters deduced from experimental data for the elastic scattering of 200 MeV protons from ^{6}Li. All potential depths are in MeV and all geometrical parameters are in fm.

V	r_0	a_0	W	r_w	a_w	V_{so}	r_{so}	a_{so}	W_{so}	r_{sow}	a_{sow}
20.6	0.80	0.36	12.1	1.20	1.31	4.1	0.44	1.05	−3.36	1.18	0.85

[a]The potential is that of Nadasen *et al.* (Ref. 78),

$$\bar{U}_0(r)=U_{\rm Coul}(r)-Vf_0(r)-iWf_w(r)+\left[2V_{so}\frac{1}{r}\frac{d}{dr}f_{so}(r)+2iW_{so}\frac{1}{r}\frac{d}{dr}f_{sow}(r)\right]l\sigma, \quad f_i(r)=\left[1+\exp\left[\frac{r-r_i}{a_i}\right]\right]^{-1} .$$

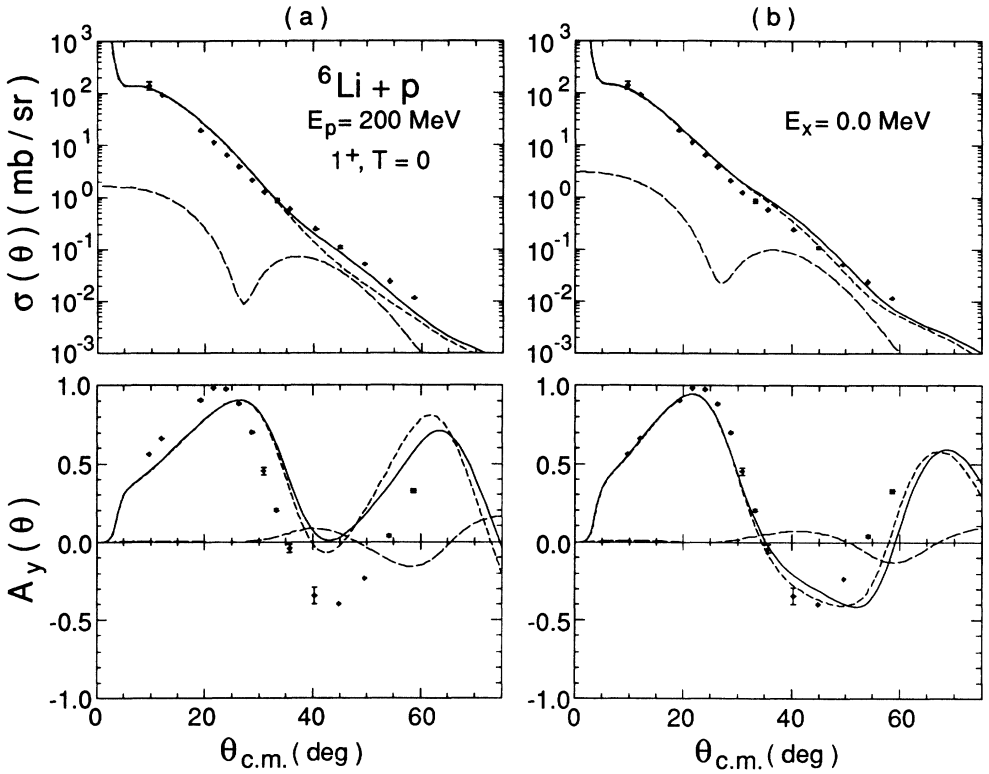

FIG. 5. The elastic scattering results obtained using the folded optical potentials based on the t-matrix and density-dependent g-matrix NN interactions are displayed in parts (a) and (b), respectively. The short dashed curve is the $J=0$ spherical term, the long-dashed curve represents the perturbative estimate of the spin-spin ($J=1$) contribution to elastic scattering, and the solid curve represents the sum of the $J=0$ and $J=1$ contributions.

partial cross sections and analyzing powers, σ^1 and A_y^1, estimated using the DWA [Eq. (15b)] and the spin-spin potential $\bar{U}_1(g,g)$ [Eq. (11)] constructed from the the first adjusted $J=1$ ground-state density set (CK with $\Delta_{12}^s=-0.217$) given in Sec. IV A are shown as long dashed curves. The summed σ and A_y are shown as solid curves.

Both microscopic folded optical potentials provide acceptable descriptions of the elastic data, although the g-matrix calculation does somewhat better. One can see from the figure that the g-matrix result for the cross section is lower (higher) at low (high) q than the t-matrix result. Note that the folded g-matrix potential provides a much better representation of the analyzing power data than does the t-matrix potential because of the shift of the first maximum and zero of the analyzing power to lower q and the improvement in the first minimum. These results can be understood from the discussion of the differences between the two effective NN interactions given in Sec. III B.

It can also be seen in Fig. 5 that the spherical term in the optical potential dominates the scattering process for momentum transfers $q \lesssim 2$ fm^{-1}. Beyond this limit the contribution from the dipole potential is small but not negligible. Results for the dipole contribution to the elastic cross section and analyzing power obtained using the second adjusted dipole density set (CK with $\Delta_{12}^s=1.00$) given in Sec. IV A differ from those shown by less than 20%. There are much larger contributions to elastic scattering observables from $J\neq 0$ potentials in ^{7}Li, ^{9}Be, and ^{10,11}B which have large quadrupole moments.[32]

B. The $3^+, T=0$; 2.184 MeV state

The inelastic differential cross section and analyzing power data for the $1^+, T=0 \rightarrow 3^+, T=0$ transition in ^{6}Li are shown in Figs. 6 and 7. Figure 6 contains DWA results with the transition potentials generated by folding the density-dependent g-matrix interaction with the LS-coupling (short-dashed curve) and phenomenological (solid curve) transition densities of Sec. IV B. In each case the distorted waves were calculated self-consistently from the folded g-matrix spherical optical potential. The calculation employing the phenomenological transition density gives an excellent reproduction of the cross section and analyzing power data. The deficiencies in the results with the LS-coupling densities are easily understood by direct comparison of Fig. 3(a) and Fig. 6. This comparison clearly demonstrates that intermediate energy protons are as sensitive as electrons to the radial shape of the transition density. This is the motivation for introducing expressions like Eq. (23) into our discussion. We discuss the differences between our results and the earlier work of Hutcheon, Sundberg, and Tibell[5] in Sec. VI.

The DWA results obtained with the density independent t-matrix and density dependent g-matrix interac-

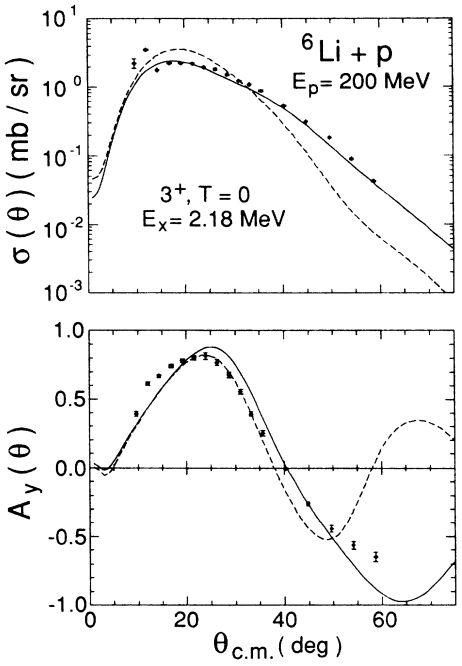

FIG. 6. The present data for the proton induced transition to the $3^+, T=0$ level in ^{6}Li is compared with DWA results based on transition potentials obtained by folding the density dependent g-matrix interaction with the LS harmonic oscillator density (dashed curve) and the phenomenological density (solid curve) given in Sec. IV B. The distortion function is generated from the g-matrix optical potential.

are compared in Fig. 7(a). The former are shown as dashed curves and the latter as solid curves. Elastic and inelastic scattering is treated self-consistently in each of these calculations, i.e., the elastic and inelastic scattering potentials are obtained with the same interaction. The $J=2$ potential was constructed from the phenomenological ρ_2^m discussed in Sec. IV B. It is evident that the density-dependent g-matrix results give an excellent representation of the cross section and analyzing power data and are clearly superior to the t-matrix results. The cross-section results indicate that the magnitude of the t matrix is slightly too large at low q (around the peak) and too small at high q. For the analyzing powers, the g matrix gives a shift to lower q of the first diffractive maxima and this shift is required by the data. These results can again be understood from our discussion on the effective interaction in Sec. III B. It may thus be concluded that effects due to Pauli blocking are important even for a diffuse nucleus such as ^{6}Li.

Effects due to the choice of distorting potential are isolated in Fig. 7(b). The three different curves represent results obtained with distortion functions [Eq. (17b)] generated from plane waves (long-dashed curve), the phenomenological WS optical potential (short-dashed curve), and the g-matrix folded optical potential (solid curve). The transition potential for all three calculations is that obtained by folding the g-matrix effective interaction with the phenomenological transition density. Distortion reduces the magnitude of the calculated cross section by about 20% and 50% at $q=1$ fm and 2 fm, respectively, relative to the plane-wave results. This is consistent with the 30–40 % reduction in magnitude at the peak of the cross section cited in Refs. 1–5, which indicates that, for ^{6}Li at these proton bombarding energies, we are approaching the plane-wave limit.

The differences due to distortion are most dramatic in the analyzing power results. These data are best described by the self-consistent g-matrix calculation. Although the g-matrix folded optical potential does not describe the elastic scattering data as well as the WS optical potential; it appears to give a better representation of the distortion experienced by the proton for this transition. In the calculations using the WS optical potential, the deficiency in the shape of the inelastic $A_y(\theta)$ at high q are due to the large radius imaginary spin-orbit term in the WS potential. It is probable that this is an artifact of subsuming the effects of the $J=1$ elastic scattering potential into the spherical optical potential.

The sensitivity of the inelastic $A_y(\theta)$ to the choice of distorting potential can be understood by considering the overlap between the transition potential and distorting function in the calculation of the transition amplitude. In general, the transition potentials tend to be localized in a particular region of r space. As a consequence of this radial localization, the form factor places more weight on the shape and magnitude of the distorting potential in the region of r space where the overlap is the greatest. In contrast, elastic scattering is averaged over the entire nuclear volume and may not adequately determine the distorting potential in such a localized region. Hence, inelastic transitions can provide a more sensitive test of the distorting potential than elastic scattering. This form of radial localization has been noticed for other nuclear systems[30,34] and has been discussed extensively by Kelly *et al.*[35]

C. The $0^+, T=1$; 3.56 MeV state

The proton scattering DWA results using the oscillator LS and adjusted CK densities for the $1^+, T=0 \rightarrow 0^+, T=1$ transition in ^{6}Li, described in Sec. IV B, are shown as the dashed and solid curves, respectively, in Fig. 8(a). The distortion function and transition potentials are calculated self-consistently with the g-matrix effective interaction. Both calculations give a reasonable description of the most forward data points, points which are subject to some uncertainty. Other more forward angle data, for the analog transition in the ^{6}Li(p,n) reaction at 200 MeV,[80] clearly favor the results obtained with the adjusted CK densities, which are also consistent with β decay.

Somewhat more interesting is the fact that the results with the LS densities do a reasonable job of giving the magnitude of the (p,p') cross section around the minimum and beyond, while the results with the adjusted CK densities significantly underestimate the cross section at the minimum. It is to be remembered that the adjusted CK densities do a better job in describing the electron scattering data than the LS densities near the minimum and beyond. The fact that the situation is reversed for

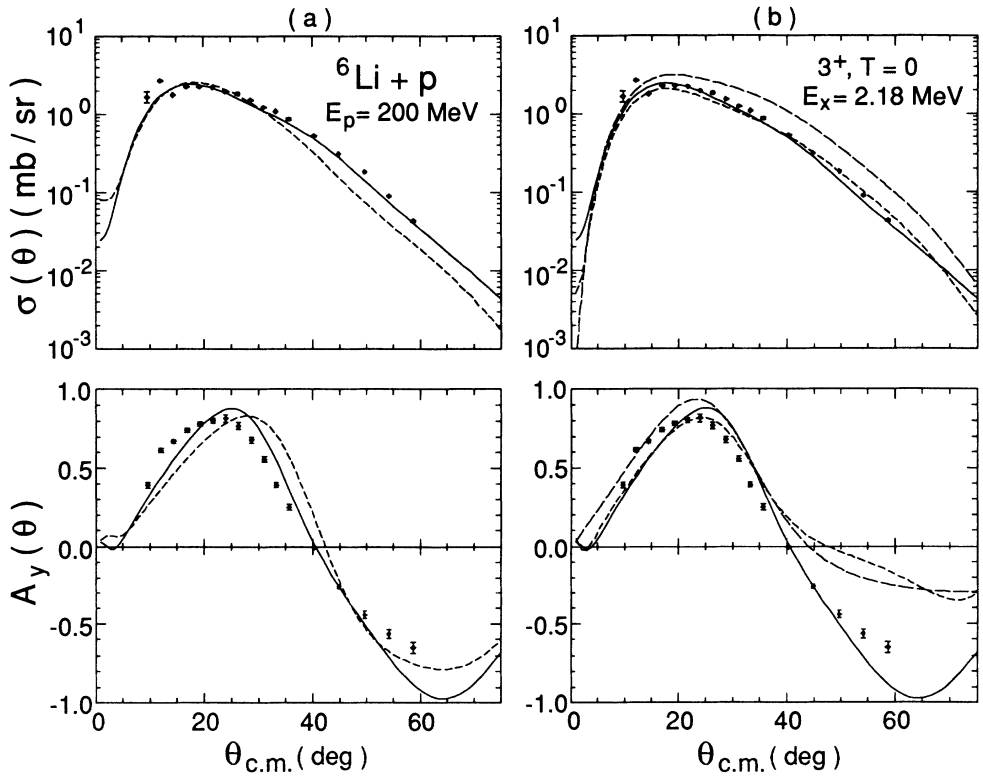

FIG. 7. Additional theoretical results for excitation of the $3^+, T=0$ state in ^{6}Li. The DWA results shown in (a) are calculated self-consistently by using the same *NN* interaction to generate the transition and optical potentials. The transition potentials are based on the phenomenological transition density. The result represented by the dashed (solid) curve are for the *t*-matrix (*g*-matrix) *NN* interaction. The DWA calculations shown in (b) use the same transition potential (*g*-matrix interaction folded with the phenomenological density) with the distortion function generated from plane waves (long-dashed), WS (short-dashed), and folded *g*-matrix (solid curve) optical potentials.

the proton scattering data indicates that the adjusted CK model spin densities are still not completely correct. This is not unexpected based on the discussion at the end of Sec. IV B above. We note that (p,p') results quite similar to the *LS* results in Fig. 8(a) are obtained by choosing $\Delta^s_{12}=0$ and $\Delta^{\bar{l}}_{12}=12.2$, which satisfies Eq. (33) and preserves the adjusted CK fit to the (e,e') data in Fig. 3(b). This result, which is shown as a solid curve in Fig. 9(b), implies that a simultaneous fit to the (p,p') and (e,e') data involves shell model configurations outside the *p* shell.

Further support for this conclusion is given in Fig. 8(b) which contains the self-consistent *g*-matrix result (solid curve) obtained with the modified radial wave-function parameters of the present work (listed in Table II). Like the adjusted CK result, these densities clearly underestimate the experimental (p,p') data in the region of the minimum and beyond. A result more consistent with the (p,p') data and conserving the fits to the (e,e') data shown in Fig. 3(b) can be obtained using the present radial wave function from Table II but taking $P^s_{12}=0.300$ and $P^{\bar{l}}_{12}=0.621$, which is consistent with Eq. (35b) but in violation of the *p*-shell constraint on the $P^{\bar{l}}_{JL}$ given in Eq. (28). This result is indicated by the dashed curve in Fig. 8(b). Although we take the results shown in Fig. 8 to be clear signatures that contributions to the dipole densities from configurations beyond the *p* shell are required, we do not wish to imply that the densities modified to better reproduce the (p,p') results above are correct, since they are still constrained to satisfy the *p*-shell relation between ρ^s_{10} and ρ^s_{12}. Rather, we are suggesting that one break this constraint with an appropriate model and determine $\rho^{s\perp}$ and $\rho^{s\parallel}$ by considering (e,e') and intermediate energy nucleon scattering data simultaneously. Such an exercise has been carried out recently for the $0^+, T=0 \rightarrow 1^+, T=1$ transition in ^{12}C.[81]

It is also important to note that all of the calculations discussed with respect to Figs. 8(a) and 8(b) give a reasonable description of the forward analyzing power ($q \leq 1.5$ fm^{-1}). In earlier work on the $0^+, T=0 \rightarrow 1^+, T=1$ ($E_x=15.11$ MeV) transition in ^{12}C, which has the same transfer quantum numbers as the $1^+, T=0 \rightarrow 0^+, T=1$ transition in ^{6}Li of interest here, Comfort *et al.*[82] noted that the forward analyzing power data were poorly described by theoretical DWIA calculations that used CK wave functions and which treated the exchange nonlocality exactly. The deficiencies in the theoretical results were subsequently attributed[62,82] to a large, non-normal transfer amplitude $LSJ=[111]$ arising from the CK wave functions which contributes to (p,p') via the exchange

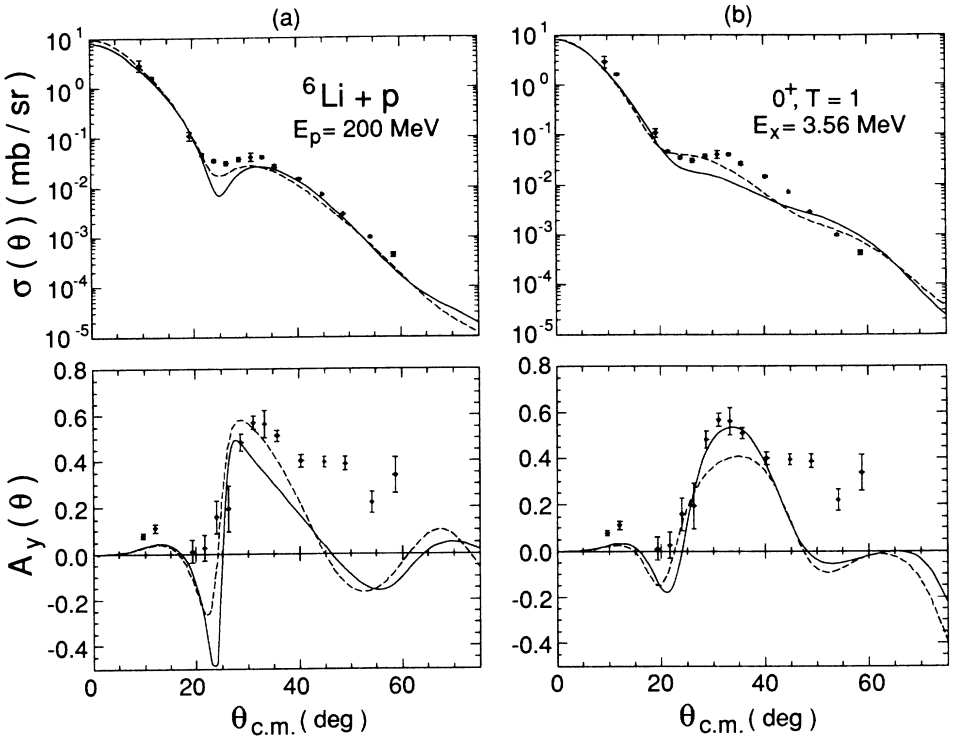

FIG. 8. The present data for the proton induced transition to the $0^+, T=1$ level in ^{6}Li is compared with DWA results based on transition potentials obtained by folding the g-matrix interaction with (a) the LS harmonic oscillator density (dashed curve) and the adjusted CK density (solid curve) and (b) the phenomenological density (solid curve) and the adjusted phenomenological density (dashed curve). The first three of these densities were specified in Sec. IV B and the last is defined in Sec. V C. For all of the results, the distortion function is generated from the g-matrix optical potential.

nonlocality and is driven by the tensor NN interaction component. It was concluded that the forward analyzing power data are sensitive to both the size of this amplitude and the strength of the tensor exchange force. Based on this work we conclude that the data for the $1^+, T=0 \rightarrow 0^+, T=1$ transition in ^{6}Li do not require the [111] amplitude since we obtain a good description of the forward analyzing powers in approximate calculations which exclude this amplitude from the outset.

To investigate the effects of changing the effective NN interaction we have performed two proton scattering calculations where the transition potentials were generated by folding t-matrix and g-matrix effective interactions with the adjusted CK density with $\Delta^s_{12}=0$. The results are shown as dashed and solid curves, respectively, in Fig. 9(a). In both of these calculations the distortion function was generated from the phenomenological WS optical potential. Thus, the differences in the calculations result entirely from the differences between these effective interactions in the $S=1$ and $T=1$ NN channel. The t-matrix cross section is lower than the g-matrix cross section at high q. The magnitude of the isovector spin-flip central t-matrix component is less than that of the g matrix at high q. At low q the two interactions and cross-section calculations are quite similar. The calculated analyzing powers are similar at low q while at larger q the t-matrix calculation is slightly higher than the g-matrix results. The differences between the t and g results are not due to density dependence (g is essentially density independent in this channel), but reflect differences in the amplitudes of Franey and Love[41] and those of the Paris potential[48] in the $S=1$, $T=1$ NN channel.

To illustrate how distortion affects the calculations, we display in Fig. 9(b) the results of calculations involving plane wave (short-dashed curve), phenomenological WS (long-dashed curve), and g-matrix folding model (solid curve) distortion functions. In each calculation the transition potential was generated by folding the g-matrix effective interaction with the adjusted CK densities with $\Delta^s_{12}=0$. We find that there is very little difference between the WS and folded g-matrix results for the cross sections, and that distortion tends to reduce the peak cross and shift the minimum to lower q relative to the plane wave result. In the case of the analyzing powers, the distortion is seen to be responsible for most of the structure in the calculations. The magnitude of the low-q oscillations from the g-matrix folding model are enhanced over those from the WS potential, while at larger q the WS calculation remains more positive and does not fall to zero as quickly as the g-matrix calcula-

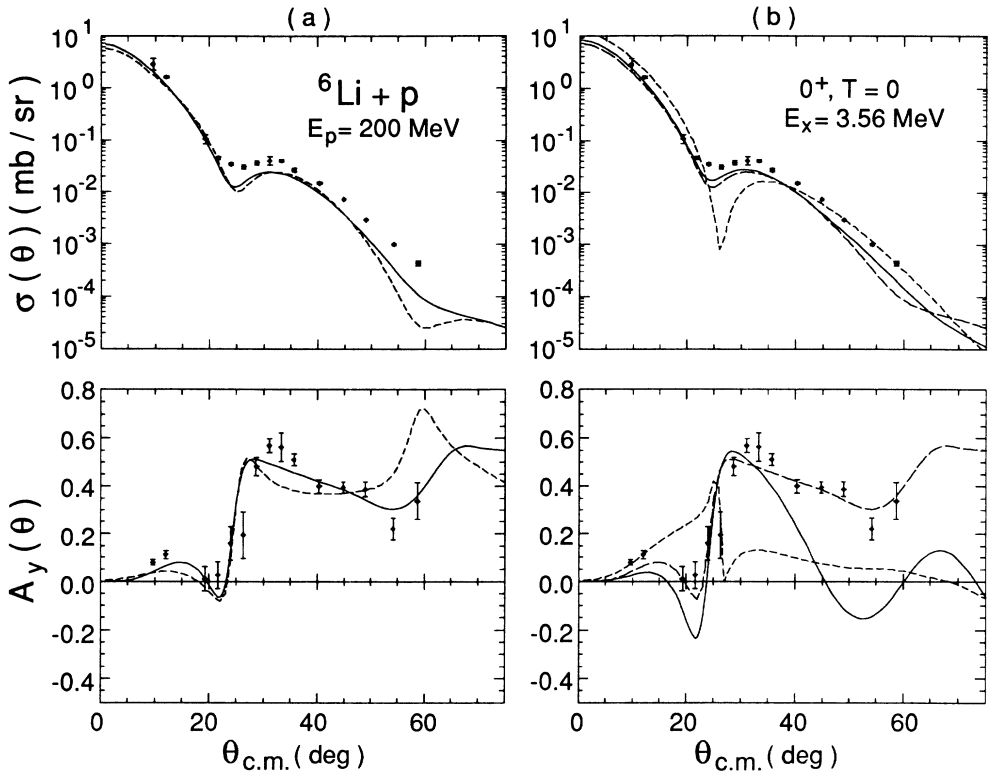

FIG. 9. Additional theoretical results for excitation of the $0^+, T=1$ state in ^{6}Li. The DWA results shown in (a) are based on transition potentials obtained by folding the t matrix (dashed curve) and the g matrix (solid curve) with the CK density with $\Delta_{12}^s=0$ described in Sec. V C. The distortion function is generated from the phenomenological WS optical potential in both cases. The results in (b) are based on the g-matrix interaction and the CK density with $\Delta_{12}^s=0$ with the distortion generated from plane waves (short-dashed), WS (long-dashed), and folded g-matrix (solid curve) optical potentials.

tion. We hesitate to conclude anything about agreement with the data at high q because of the questions voiced above regarding the imaginary WS spin-orbit potential.

VI. SUMMARY AND CONCLUSIONS

We began this paper by referring to the work of Hutcheon, Sundberg, and Tibell,[5] who computed PWIA and DWIA cross sections for 185 MeV (p,p') reactions for the $1^+, T=0 \rightarrow 3^+, T=0$ and $0^+, T=1$ transitions in ^{6}Li based on electromagnetic data. The calculations overestimated the experimental cross sections by factors of 3 and 2, respectively. We have presented here new 200 MeV $(\vec{p},p)$ and $(\vec{p},p')$ data and examined many of the features of the effective NN interaction and the structure of ^{6}Li not considered in Ref. 5. These were indicated in items (ii) and (iii) of the Introduction.

Specifically, we made detailed single scattering model calculations based on free and Pauli-corrected effective NN interactions with the nuclear structure input constrained by a comprehensive set of weak and electromagnetic data. A very good overall description of the data was achieved, particularly in the case of the observables associated with natural parity amplitudes. Although the improvement in the results obtained is due, in part, to the properties of the Pauli-corrected interactions, the most important differences between the present calculations and those of Ref. 5 have to do with the nuclear structure assumptions.

The discussion of Ref. 5 is based on PWA expressions equivalent to Eq. (23) above. In relating the $3^+(p,p')$ data to electron scattering, they assume that ρ_2^s/ρ_2^m, $\rho_2^{s\parallel}/\rho_2^m$, and $\rho_2^{s\perp}/\rho_2^m$ are as given by the LS-coupling shell model (Table I). Core polarization considerations,[10,83] coupled with the experimental indication of a small transverse form factor for this transition[11,14,18,20] suggest that these ratios should be much smaller than indicated by the LS-coupling model. We have set them to zero in the present calculations. This difference is the primary source of the large decrease of the predicted $3^+(p,p')$ cross section relative to Ref. 5.

For the 0^+ excitation, Ref. 5 attempted to relate the (p,p') and (e,e') data via the pure LS-coupling amplitudes (again Table I). The difficulties with this assumption are clearly spelled out in Sec. V C above and do lead to an apparent overestimation of the (p,p') cross-section data. In the discussion of the $1^+, T=0 \rightarrow 0^+, T=1$ transition, it was emphasized that weak, electromagnetic, and nucleon scattering data are needed simultaneously to pin down the nuclear structure. Of these, nucleon scattering is the essential source of information on the longitudinal spin transition densities.

ACKNOWLEDGMENTS

Supported in part by ORNL, which is operated by Martin Marietta Energy Systems, Inc., under Contract

No. DE-AC05-84OR214000 with the U.S. Department of Energy, IUCF, which is supported in part by the National Science Foundation, and the Florida State University Supercomputer Computations Research Institute, which is partially funded by the U.S. Department of Energy through Contract No. DE-FC05-85ER250000. We also acknowledge the timely assistance of Julia Smith, University of Arkansas, who was a Summer Undergraduate Research Fellow under the NSF-REU program Grant No. PHY-89-04777 at Florida State University.

---

*Present address: Oak Ridge National Laboratory, Oak Ridge, TN 37831.

†Present address: Los Alamos National Laboratory, Los Alamos, NM 87545.

‡Present address: University of Kentucky, Lexington, KY 40506.

§Present address: Austin Peay State University, Clarksville, TN 37044.

[1]D. F. Jackson, Nucl. Phys. **35**, 194 (1962).

[2]D. F. Jackson and J. Mahalanabis, Nucl. Phys. **64**, 97 (1965).

[3]D. Hasselgren, P. U. Renberg, O. Sundberg, and G. Tibell, Nucl. Phys. **69**, 1 (1965).

[4]B. Geoffrion, N. Marty, M. Morlet, B. Tatischeff, and A. Willis, Nucl. Phys. **A116**, 209 (1968).

[5]R. M. Hutcheon, O. Sundberg, and G. Tibell, Nucl. Phys. **A154**, 261 (1970).

[6]S. M. Austin and G. M. Crawley, Phys. Lett. **27B**, 570 (1968).

[7]S. S. Mani, D. Jacques, and A. D. B. Dix, Nucl. Phys. **A165**, 145 (1971); **A172**, 166 (1971).

[8]K. H. Bray, M. Jain, K. S. Jayaraman, G. Lobianco, G. A. Moss, W. T. H. Van Oers, D. O. Wells, and F. Petrovich, Nucl. Phys. **A189**, 35 (1972).

[9]R. S. Henderson, S. F. Collins, B. M. Spicer, G. G. Shute, V. C. Officer, D. W. Devins, D. L. Friesel, and W. P. Jones, Nucl. Phys. **A372**, 117 (1981).

[10]F. Petrovich, R. H. Howell, C. H. Poppe, S. M. Austin, and G. M. Crawley, Nucl. Phys. **A383**, 355 (1982).

[11]M. Bernheim and G. R. Bishop, Phys. Lett. **5**, 270 (1963); U. S. Neudatchin and Yu. I. Smirnov, Prog. Nucl. Phys. **10**, 273 (1969).

[12]R. M. Hutcheon, T. E. Drake, V. W. Stobie, G. A. Beer, and H. S. Caplan, Nucl. Phys. **A107**, 266 (1968).

[13]L. R. Suelzle, M. R. Yearian, and H. Crannell, Phys. Rev. **162**, 992 (1967).

[14]G. C. Li, I. Sick, R. R. Whitney, and M. R. Yearian, Nucl. Phys. **A162**, 583 (1971).

[15]R. E. Rand, R. Frosch, and M. R. Yearian, Phys. Rev. **144**, 859 (1966).

[16]J. C. Bergstrom, S. B. Kowalski, and R. Neuhausen, Phys. Rev. C **25**, 1156 (1982).

[17]R. Neuhausen, Z. Phys. **220**, 456 (1969).

[18]R. Eigenbrod, Z. Phys. **228**, 337 (1969).

[19]R. Yen, L. S. Cardman, D. Kalinsky, J. R. Legg, and C. K. Bockelman, Nucl. Phys. **A235**, 135 (1974).

[20]J. C. Bergstrom and E. I. Tomusiak, Nucl. Phys. **A262**, 196 (1976).

[21]R. Neuhausen and R. M. Hutcheon, Nucl. Phys. **A164**, 497 (1971).

[22]J. C. Bergstrom, I. P. Auer, and R. S. Hicks, Nucl. Phys. **A251**, 401 (1975).

[23]J. C. Bergstrom, U. Deutschmann, and R. Neuhausen, Nucl. Phys. **A327**, 439 (1979).

[24]J. C. Bergstrom, Nucl. Phys. **A327**, 458 (1979).

[25]A. K. Kerman, H. McManus, and R. M. Thaler, Ann. Phys. (N.Y.) **8**, 551 (1959).

[26]F. Petrovich and W. G. Love, Nucl. Phys. **A354**, 499c (1981).

[27]F. Petrovich, J. A. Carr, and H. McManus, Annu. Rev. Nucl. Part. Sci. **36**, 29 (1986).

[28]W. N. Hess, Rev. Mod. Phys. **30**, 369 (1958).

[29]C. Olmer, A. D. Bacher, G. T. Emery, W. P. Jones, D. W. Miller, H. Nann, P. Schwandt, S. Yen, T. E. Drake, and R. J. Sobie, Phys. Rev. C **29**, 361 (1984).

[30]C. W. Glover *et al.*, unpublished data and analysis for 200-MeV proton scattering from ^{16}O.

[31]V. Comparat, R. Frascaria, N. Fujiwara, N. Marty, M. Morlet, P. G. Roos, and A. Willis, Phys. Rev. C **12**, 251 (1975).

[32]A. W. Carpenter, F. Petrovich, R. J. Philpott, and J. A. Carr (unpublished).

[33]J. R. Comfort and B. C. Karp, Phys. Rev. C **21**, 2162 (1980).

[34]J. Kelly, W. Bertozzi, T. N. Buti, F. W. Hersman, C. Hyde, M. V. Hynes, B. Norum, F. N. Rad, A. D. Bacher, G. T. Emery, C. C. Foster, W. P. Jones, D. W. Miller, B. L. Berman, W. G. Love, and F. Petrovich, Phys. Rev. Lett. **45**, 2012 (1980).

[35]W. Bertozzi, T. N. Buti, J. M. Finn, F. W. Hersman, C. Hyde-Wright, M. V. Hynes, M. A. Kovash, B. Murdock, B. E. Norum, B. Pugh, F. N. Rad, A. D. Bacher, G. T. Emery, C. C. Foster, W. P. Jones, D. W. Miller, B. L. Berman, W. G. Love, J. A. Carr, and F. Petrovich, Phys. Rev. C **39**, 1222 (1989); J. Kelly, Ph.D. thesis, Massachusetts Institute of Technology, 1981 (unpublished).

[36]M. Hugi, W. Bauhoff, and H. O. Meyer, Phys. Rev. C **28**, 1 (1983).

[37]L. Rikus, K. Nakano, and H. V. von Geramb, Nucl. Phys. **A414**, 413 (1984).

[38]G. E. Brown, in *Spin Excitations in Nuclei,* edited by F. Petrovich *et al.* (Plenum, New York, 1984), p. 233.

[39]W. G. Love, M. A. Franey, and F. Petrovich, in *Spin Excitations in Nuclei* (Ref. 38), p. 205.

[40]R. A. Lindgren and F. Petrovich, in *Spin Excitations in Nuclei* (Ref. 38), p. 323.

[41]M. A. Franey and W. G. Love, Phys. Rev. C **31**, 488 (1985).

[42]J. P. Jeukenne, A. Lejeune, and C. Mahaux, Phys. Rev. C **10**, 1931 (1974); **15**, 10 (1977); **16**, 80 (1977).

[43]F. A. Brieva and J. R. Rook, Nucl. Phys. **A291**, 299 (1977); **A291**, 317 (1977); **A297**, 206 (1978); **A307**, 493 (1978).

[44]H. V. von Geramb, F. A. Brieva, and J. R. Rook, in *Microscopic Optical Potentials* (Lecture Notes in Physics No. 89), edited by H. V. von Geramb (Springer, Berlin, 1979), p. 104.

[45]H. V. von Geramb, in *The Interaction Between Medium Energy Nucleons in Nuclei* (AIP Conf. Proc. No. 97), edited by H. O. Meyer (AIP, New York, 1983), p. 44.

[46]H. V. von Geramb and W. Bauhoff, Tables of Effective Density and Energy Dependent Interactions for Nucleons, Universitat Hamburg report (unpublished).

[47]K. A. Brueckner, J. L. Gammel, and H. Weitzner, Phys. Rev. **110**, 1023 (1958); K. A. Brueckner, A. M. Lockett, and R. Rotenberg, *ibid.* **121**, 255 (1961); J. W. Negele, Phys. Rev. C **1**, 1260 (1970).

[48]M. Lacombe, B. Loiseau, J. M. Richard, R. Vinh Mau, J. Côté, P. Pirès, and R. de Tourreil, Phys. Rev. C **21**, 861 (1980).

[49]S. Cohen and D. Kurath, Nucl. Phys. **73**, 1 (1965); T.-S. Lee and D. Kurath, Phys. Rev. C **21**, 293 (1980).
[50]F. Ajzenberg-Selove, Nucl. Phys. **A320**, 1 (1979).
[51]G. H. Fuller and V. W. Cohen, Nucl. Data **A5**, 433 (1969).
[52]P. Schwandt, H. O. Meyer, W. W. Jacobs, A. D. Bacher, S. E. Vigdor, M. D. Kaitchuck, and T. R. Donoghue, Phys. Rev. C **26**, 55 (1982).
[53]S. M. Grimes, P. Grabmays, J. O'Donnell, and R. Mozer, PEAKFIT, Ohio University, 1979 (unpublished).
[54]See AIP document no. PAPS PRVCA-41-2487-4 for 4 pages containing a complete tabulation of the data described in this paper. Order by PAPS number and journal reference from American Institute of Physics, Physics Auxiliary Publication Service, 335 East 45th Street, New York, NY 11017. The prepaid price is $1.50 for a microfiche, or $5.00 for a photocopy. Airmail additional.
[55]G. R. Satchler, *Direct Nuclear Reactions* (Oxford University, Oxford, 1983).
[56]R. G. Newton, *Scattering Theory of Waves and Particles* (McGraw Hill, New York, 1966), p. 218.
[57]F. Petrovich, H. McManus, V. Madsen, and J. Atkinson, Phys. Rev. Lett. **22**, 895 (1969).
[58]W. G. Love, Nucl. Phys. **A312**, 160 (1978).
[59]F. Petrovich, in *Microscopic Optical Potentials* (Ref. 44), p. 155.
[60]S. L. Tabor, G. Neuschaefer, J. A. Carr, F. Petrovich, C. C. Chang, A. Guterman, M. T. Collins, D. L. Friesel, C. Glover, S. Y. van der Werf, and S. Raman, Nucl. Phys. **A422**, 12 (1984). The Appendix to this paper contains the complete argument, including explicit expressions for v_{pt} and $\bar{v}_{pt}$, for the caes of ^{3}He- and t-nucleus scattering. These are easily reduced to the nucleon-nucleus scattering case.
[61]F. Petrovich, J. A. Carr, R. J. Philpott, and A. W. Carpenter, Phys. Lett. B **207**, 1 (1988).
[62]W. G. Love and J. R. Comfort, Phys. Rev. C **29**, 2135 (1984).
[63]F. Petrovich, Nucl. Phys. **A251**, 143 (1975).
[64]F. Petrovich, R. J. Philpott, A. W. Carpenter, and J. A. Carr, Nucl. Phys. **A425**, 609 (1984).
[65]J. A. Carr, F. Petrovich, D. Halderson, and J. Kelly, Computer program ALLWRLD (unpublished).
[66]J. A. Carr, F. Petrovich, D. Halderson, and J. Kelly, version of the computer program TAMURA (unpublished), based on an early version of the code VENUS by T. Tamura, W. R. Coker, and F. Rybicki, Comput. Phys. Commun. **2**, 94 (1971).
[67]A. W. Carpenter, Computer program EFIT (unpublished).
[68]J. J. Kelly, in *The Interaction Between Medium Energy Nuclei* (Ref. 45), p. 153.
[69]J. J. Kelly and J. A. Carr, in *Spin Excitations in Nuclei* (Ref. 38), p. 253.
[70]The relationship between the zero in the analyzing power and the zero in the spin-independent central interaction component is discussed in S. Yen, R. J. Sobie, T. E. Drake, A. D. Bacher, G. T. Emery, W. P. Jones, D. Miller, C. Olmer, P. Schwandt, W. G. Love, and F. Petrovich, Phys. Lett. **165B**, 421 (1981).
[71]T. A. Griffy and D. U. L. Yu, Phys. Rev. **139**, B880 (1965).
[72]T. de Forest and J. D. Walecka, Adv. Phys. **15**, 1 (1966).
[73]L. J. Tassie and F. C. Barker, Phys. Rev. **111**, 940 (1958).
[74]See, for example, P. Blunden, B. Castel, and H. Toki, Nucl. Phys. **A440**, 647 (1985). Further information may be obtained from individual papers by A. Arima, I. S. Towner, and F. C. Khanna, and W. Weise and A. Härting, in *Spin Excitations in Nuclei* (Ref. 38), pp. 7, 131, and 173, respectively.
[75]H. S. Wilson, R. W. Kavanaugh, and F. M. Mann, Phys. Rev. C **22**, 1696 (1980).
[76]R. R. Kiziah, M. D. Brown, C. J. Harvey, D. S. Oakley, D. P. Saunders, P. A. Seidl, C. F. Moore, W. B. Cottingame, R. W. Garrnett, S. J. Greene, G. A. Luna, G. R. Burleson, and D. B. Holtkamp, Phys. Rev. C **30**, 1643 (1984).
[77]J. Rapaport, D. Wang, J. A. Carr, F. Petrovich, C. C. Foster, C. D. Goodman, C. Gaarde, J. Larsen, C. A. Goulding, T. N. Taddeucci, D. Horen, and E. Sugarbaker, Phys. Rev. C **36**, 500 (1987).
[78]A. Nadasen, P. Schwandt, P. P. Singh, W. W. Jacobs, A. D. Bacher, P. T. Debevec, M. D. Kaitchuck, and M. T. Meek, Phys. Rev. C **23**, 1023 (1981).
[79]P. Schwandt, Computer program SNOOPY, Indiana University Cyclotron Facility Report No. 82-3 (1982).
[80]J. Rapaport, C. C. Foster, C. D. Goodman, C. A. Goulding, T. N. Taddeucci, D. Horen, E. Sugarbaker, C. Gaarde, J. Larsen, J. A. Carr, F. Petrovich, and M. J. Threapleton, Phys. Rev. C **41**, 1920 (1990).
[81]J. A. Carr and F. Petrovich, unpublished results.
[82]J. R. Comfort, G. L. Moake, C. C. Foster, P. Schwandt, and W. G. Love, Phys. Rev. C **26**, 1800 (1982).
[83]F. Petrovich, J. Borysowicz, H. McManus, and G. R. Hammerstein, Phys. Rev. C **16**, 839 (1977).